Lithos 119 (2010) 123–136

Contents lists available at ScienceDirect

Lithos

journal homepage: www.elsevier.com/locate/lithos

Flood basalt-related Fe–Ti oxide deposits in the Emeishan large igneous province, SW China

Kwan-Nang Pang [a,*], Mei-Fu Zhou [a], Liang Qi [b], Gregory Shellnutt [c], Christina Yan Wang [d], Donggao Zhao [e]

[a] Department of Earth Sciences, The University of Hong Kong, Hong Kong, China
[b] State Key Lab of Ore Deposit Geochemistry, Institute of Geochemistry, Chinese Academy of Sciences, Guiyang 550002, China
[c] Academia Sinica, Institute of Earth Sciences, 128 Academia Road Sec. 2, Nankang, Taipei 11529, Taiwan
[d] Guangzhou Institute of Geochemistry, Chinese Academy of Sciences, Guangzhou 510460, China
[e] Department of Geological Sciences, Jackson School of Geosciences, The University of Texas at Austin, 1 University Station C1100, Austin, TX 78712, USA

ARTICLE INFO

Article history:
Received 13 November 2009
Accepted 16 June 2010
Available online 28 June 2010

Keywords:
Emeishan
Flood basalt
Fe–Ti oxide ore
Layered intrusion
Panxi

ABSTRACT

In the Panzhihua–Xichang region (Sichuan Province, SW China), there are a number of world-class magmatic Fe–Ti oxide deposits. They are hosted as conformable masses in lower parts of layered mafic–ultramafic intrusions that are part of the end-Guadalupian (~260 Ma) Emeishan large igneous province. The ore-bearing Panzhihua, Hongge, Baima, Taihe and Xinjie intrusions are spatially and temporally associated with flood basalts and granitoids in the province. New mineralogical data for Fe–Ti oxide ores in the Hongge and Baima intrusions, combined with an overview of previously published data, provide a better understanding on the formation of these enigmatic deposits. Geochemical and Sr–Nd isotopic data confirm a genetic relation between the intrusions and high-Ti Emeishan flood basalts. Parental magma compositions, estimated using the most Mg-rich cumulus olivine in the intrusions, are characterized by slight to moderate degrees of fractionation (MgO = 7.2–11 wt.%). Occurrences of rare Cr-bearing titanomagnetite (Cr_2O_3 = 1.2–10.7 wt.%) in the Panzhihua, Hongge and Xinjie intrusions are consistent with early crystallization of Fe–Ti oxides. Oxide-silicate equilibria and low V concentration (<4800 ppm) in magnetite are consistent with relatively high oxygen fugacity. Flood basalt-related origin, early Fe–Ti oxide crystallization and relatively high oxygen fugacity, are characteristic of Fe–Ti oxide deposits in the Panxi region but are fundamentally different from those hosted in highly-differentiated, upper parts of large layered intrusions (e.g. the Bushveld Complex). Similar Fe–Ti oxide deposits have not been documented in other well-studied large igneous provinces to date, but a number of Fe–Ti oxide ore occurrences worldwide are potentially similar to this type of flood basalt-related oxide deposits.

1. Introduction

Global magmatic Fe–Ti oxide deposits are associated with mafic intrusions or Proterozoic anorthosite complexes and form by the concentration of Fe–Ti oxides in gabbroic or ferrodioritic magma chambers (Lister, 1966; Force, 1991). No such deposits were related to flood basalts in large igneous provinces (LIPs) in the past, until the recent discovery that many of the Fe–Ti oxide deposits in the Panzhihua–Xichang (Panxi) region, SW China, are related to the ~260 Ma Emeishan LIP (Zhong et al., 2005; Zhou et al., 2008). Oxide ores hosted as extensive conformable masses in layered mafic–ultramafic intrusions represent world-class resources of Fe, Ti and V (Ma et al., 2001, 2003). These enigmatic oxide deposits have attracted a substantial number of petrologic and geochemical studies, but most of them are based on individual deposits as case studies (Zhong et al., 2002, 2003; Zhou et al., 2005; Pang et al., 2008a,b, 2009; Wang et al., 2008; Shellnutt et al., 2009). However, this group of deposits has not been compared with magmatic Fe–Ti oxide deposits worldwide. Thus, it is unknown if they represent a new type of Fe–Ti oxide deposits. Likewise, their significance for mineral exploration elsewhere is not clear. This contribution aims to fill this research gap by placing all published geochemical data together as a single database. In addition, we provide mineralogical and geochemical data for Fe–Ti oxide ores in the Hongge and Baima intrusions. The combined datasets give us a better understanding on the key features and formation of this group of deposits. Our results reveal that the flood basalt-related Fe–Ti oxide deposits in the Panxi region are different in many aspects compared to those hosted in highly-differentiated, upper portions of large layered intrusions (e.g. the Bushveld Complex) (Cawthorn and Molyneux, 1986; Tegner et al., 2006). We propose that the Fe–Ti oxide deposits in the Panxi region represent another important class of magmatic Fe–Ti oxide deposits.

* Corresponding author. Present address: Department of Geosciences, National Taiwan University, Taipei P.O. Box 13-318, Taipei 10699, Taiwan. Tel.: +886 2 33662924; fax: +886 2 23636095.
E-mail address: knpang@graduate.hku.hk (K.-N. Pang).

0024-4937/$ – see front matter © 2010 Elsevier B.V. All rights reserved.
doi:10.1016/j.lithos.2010.06.003

2. The Emeishan LIP and associated Fe–Ti oxide deposits

The Emeishan LIP is located geographically in the Sichuan, Guizhou and Yunnan provinces, SW China and tectonically at the eastern margin of the Yangtze Block and the western margin of the Tibetan Plateau (SBGMR, 1991; Chung and Jahn, 1995; Ali et al., 2005) (Fig. 1). The province is dominated by flood basalts (the Emeishan flood basalts) ranging in thickness from a few hundred meters to a maximum of ~5 km. Erosional remains of the flood basalts cover an area of at least 2.5×10^5 km^2. The flood basalts were likely emplaced at or close to sea level (Thompson et al., 2001; Ukstins Peate and Bryan, 2009). Similar to many continental flood basalts, the Emeishan flood basalts include high-Ti and low-Ti lavas (Xu et al., 2001; Xiao et al., 2004). Biostratigraphic data from the Permian limestone on which the lavas erupted, paleomagnetic data of the volcanic succession, and radiometric dating of a feeder intrusion to the basalts constrain the age of the province at ~260 Ma, synchronous with the end-Guadalupian mass extinction (Ali et al., 2002; Zhou et al., 2002).

The Panxi region lies in the central-western part of the Emeishan LIP where the flood basalts are variably deformed, uplifted and eroded due to strong tectonic activity in the Cenozoic. Magmatic Fe–Ti oxide deposits are documented in several layered intrusions in this region whose exposure is controlled by major N–S trending faults. The deposits and host layered intrusions follow the same names including Panzhihua, Hongge, Baima, Taihe and Xinjie. Most of the intrusions have been dated by U–Pb zircon radiometric method at ~260 Ma (Fig. 2). The ore-bearing intrusions are spatially associated with contemporaneous flood basalts and copious granitoids (Zhang et al., 1999; Ma et al., 2001). Four major Fe–Ti oxide deposits including Panzhihua, Hongge, Baima and Xinjie account for a total ore reserve of ~7209 Mt total Fe, ~559 Mt TiO_2 and ~17.4 Mt

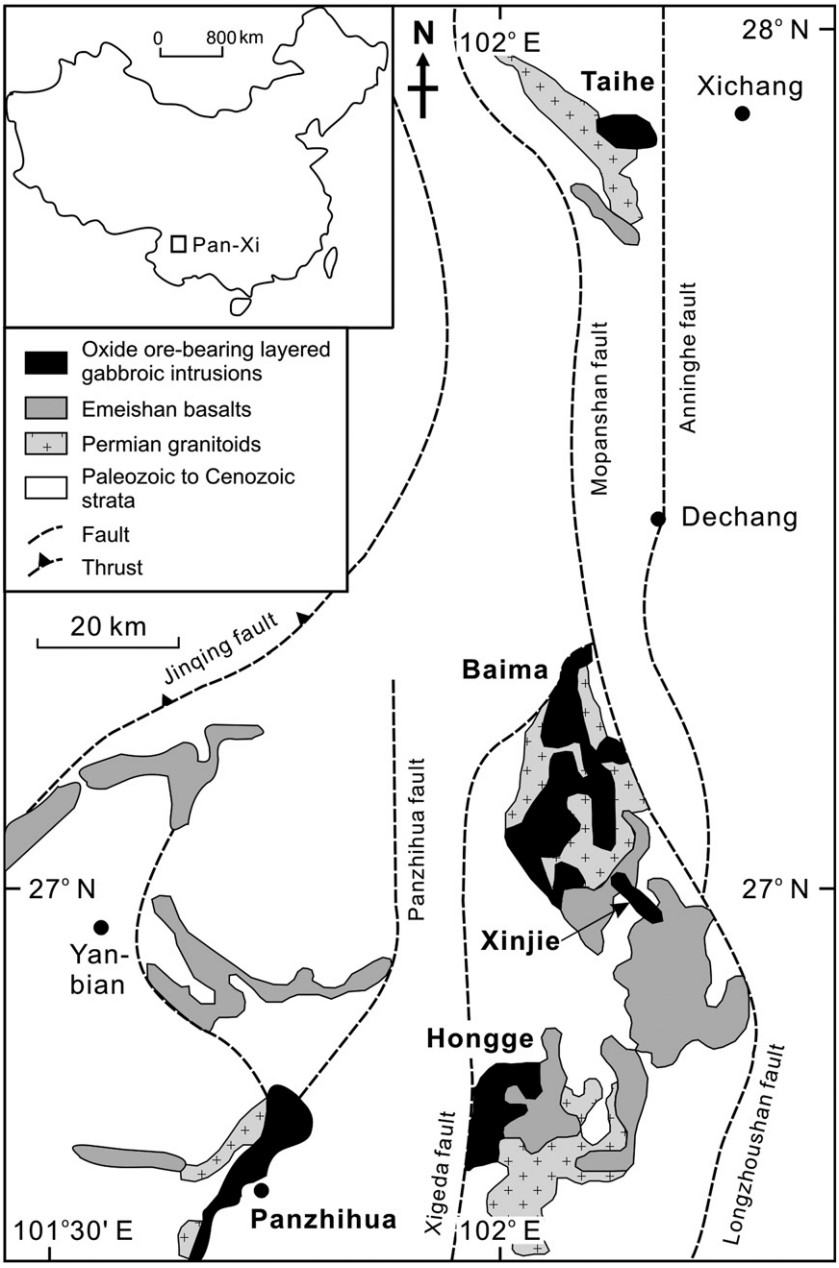

Fig. 1. Simplified geological map of the Panxi region, SW China showing the locations of the Fe–Ti oxide ore-bearing layered intrusions (modified after Liu et al., 1985).

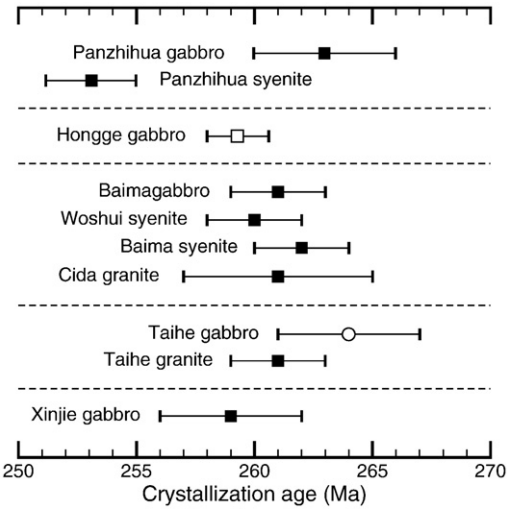

Fig. 2. Summary of U–Pb zircon ages from Fe–Ti oxide ore-bearing layered intrusions and associated granitoids in the Panxi region (SW China). Filled squares = analyses by sensitive high-resolution ion microprobe, empty squares = analyses by isotope-dilution thermal ionization mass spectrometry, empty circle = analyses by laser-ablation inductively coupled plasma mass spectrometry. Sources: Zhou et al. (2002), Zhou et al. (2005), Luo et al. (2006), Zhong and Zhu (2006), Shellnutt and Zhou (2007), Zhong et al. (2007), Zhou et al. (2008), Shellnutt et al. (2009), Zhong et al. (2009).

V_2O_5 (Ma et al., 2003; Zhong et al., 2005). The ores are concentrated, smelted and purified to TiO_2, which is used for white pigments.

3. Geology and stratigraphy of the ore-bearing intrusions

3.1. Panzhihua intrusion

The Panzhihua intrusion (26°35′N, 101°40′E) is a 19-km-long and 2-km-thick gabbroic sill with exposed area of ~30 km^2. The Panzhihua Fe–Ti–(V) oxide deposit was discovered between 1936 and 1940 (Ma et al., 2003); mining activity commenced in 1967 and is still ongoing at the present day. The intrusion contains 1333 Mt of ore reserve with a mean grade of ~33% total Fe, ~12% TiO_2 and ~0.3% V_2O_5 (Ma et al., 2003). It was dated using sensitive high-resolution ion microprobe (SHRIMP) U–Pb zircon method at 263 ± 3 Ma (Zhou et al., 2005). The intrusion was cut by faults into fault-bounded blocks, but remains largely intact, unmetamorphosed and undeformed. It was emplaced into Neoproterozoic dolomitic limestone (Dengying Formation) and resulted in the formation of a ~300-m-thick metamorphic aureole consisting of marble and skarns along its lower contact (Ganino et al., 2008). The intrusion is divided from the base upwards into the Marginal zone (MGZ), Lower zone (LZ), Middle zone (subzones MZa and MZb) and Upper zone (UZ) (Fig. 3). Igneous layering is well-developed in the MZa, MZb and UZ and dips northwest at medium to high angles. The MGZ is a hornblende-rich unit composed mainly of microgabbros suggested to be the chilled base of the intrusion. The LZ and MZa consist of gabbroic (Fig. 4a), oxide gabbroic, and Fe–Ti oxide cumulates with varying amounts of olivine, clinopyroxene, plagioclase and titanomagnetite (oxy-exsolved into magnetite and ilmenite). The MZb consists of leucogabbroic cumulates with apatite and ilmenite in addition to the above cumulus assemblage and olivine is present throughout this zone. The UZ is dominated by gabbroic cumulates with the same cumulus assemblage

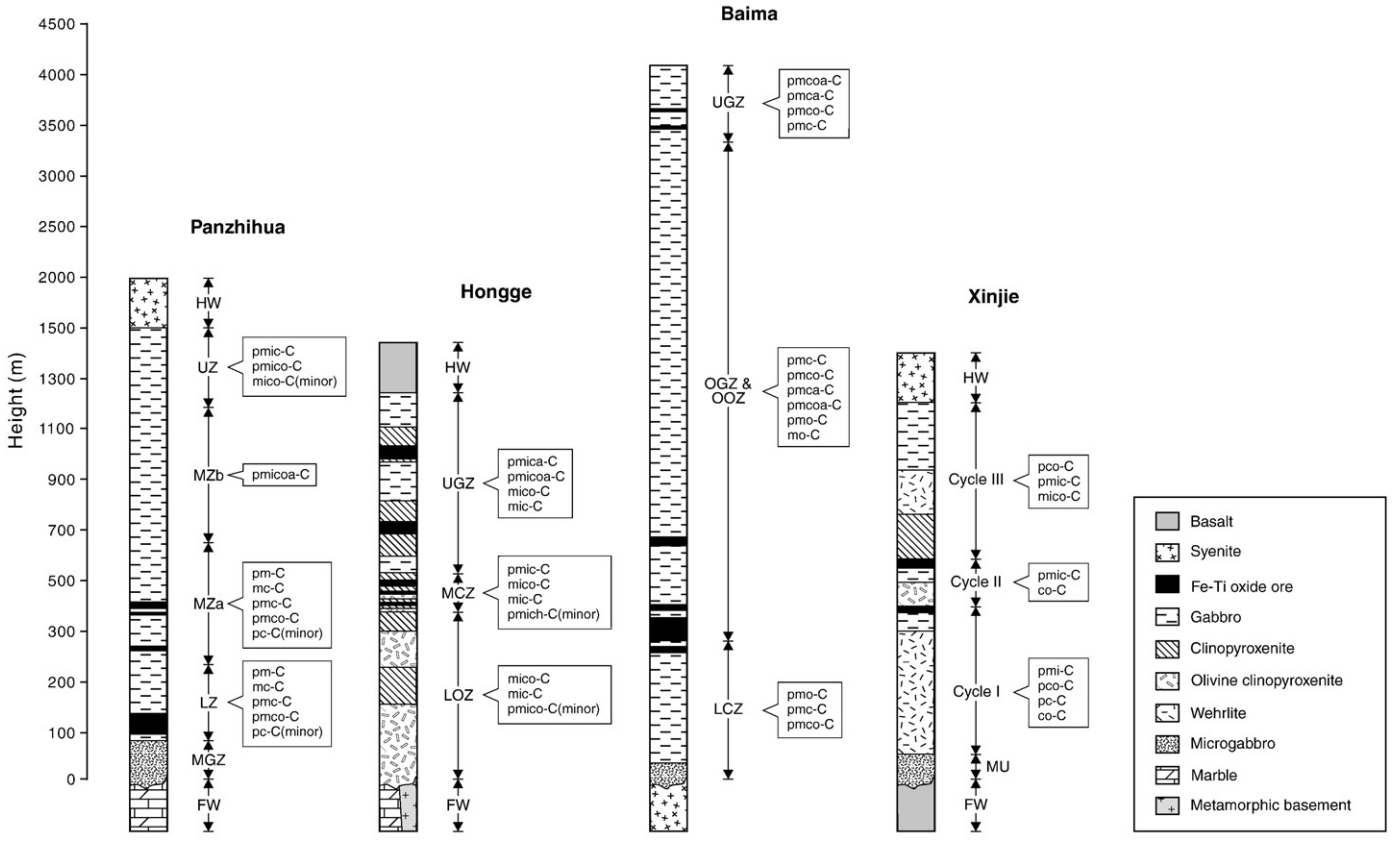

Fig. 3. Simplified stratigraphy of the Panzhihua, Hongge, Baima and Xinjie intrusions. The Irvine (1982) nomenclature was used by which rocks are named according to the first letter of the main minerals followed by "−C" meaning cumulus. These minerals include plagioclase(p), magnetite(m), ilmenite(i), clinopyroxene(c), orthopyroxene(h), olivine(o) and apatite(a). Note the vertical exaggeration to illustrate the details of the ore-bearing part of the intrusions. FW = footwall, HW = hangingwall. See text for the abbreviated stratigraphic zones.

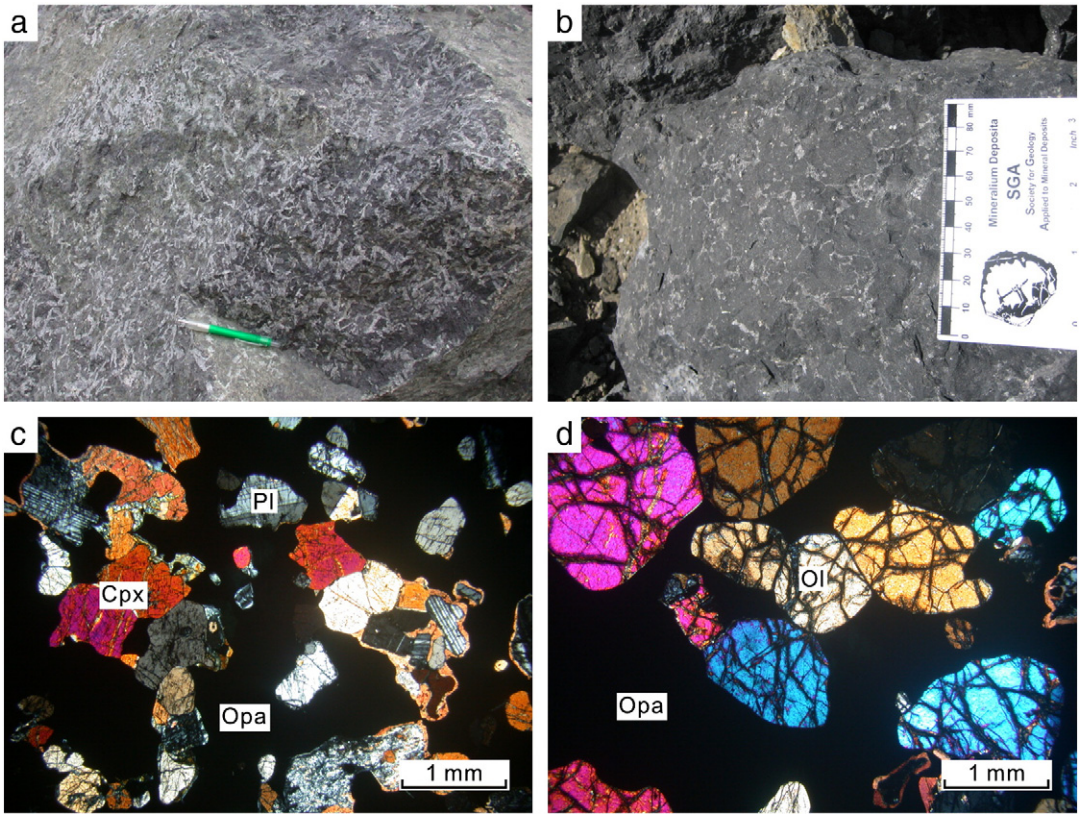

Fig. 4. Field and petrographic features of oxide ores and host rocks of the ore-bearing intrusions. a. Gabbroic cumulate (pmc-C) in the Panzhihua intrusion consisting of plagioclase and clinopyroxene with sub-ordinate amount of Fe–Ti oxides. b. Olivine-rich cumulate (mico-C) in the Hongge intrusion consisting of dark olivine aggregates. c. Photomicrograph of Fe–Ti oxide ore sample (pmc-C) from the Panzhihua intrusion (ZJ02). d. Photomicrograph of Fe–Ti oxide ore sample (mo-C) from the Baima intrusion (GS04-039). Similar mineralogy in terms of silicate phases between the ores and host rocks indicates a magmatic origin of the ores. Mineral symbols: Cpx = clinopyroxene, Ilm = ilmenite, Ol = olivine, Opa = opaque oxides.

as LZ and MZa. Oxide ores occur as conformable lenses and layers, up to ~60-m-thick, in the MGZ, LZ and lower MZa, either in sharp or gradational contacts against their host rocks. Contemporaneous granitoids crop out to the northwest of, sub-parallel to, and thus structurally above the intrusion (Shellnutt and Zhou, 2007; Zhong et al., 2009). Field evidence suggests that they intruded the Emeishan flood basalts further to the west.

3.2. Hongge intrusion

The Hongge intrusion (26°39′N, 101°59′E) is a layered lopolith with an exposed area of ~60 km^2 and thickness of ~1.7 km. The Hongge Fe–Ti–(V) oxide deposit was explored between 1966 and 1980, but has not been mined at a large-scale in the past. The estimated ore reserve is 4572 Mt with a mean grade of ~27% total Fe, ~11% TiO_2 and ~0.24% V_2O_5 (Ma et al., 2003). The intrusion was dated using the isotope-dilution thermal ionization mass spectrometry U–Pb zircon method at 259.3 ± 1.3 Ma (Zhong and Zhu, 2006). It was emplaced into Neoproterozoic dolomitic limestone (Dengying Formation) and Precambrian basement rocks, and is divided from the base upwards into the lower olivine clinopyroxenite zone (LOZ), middle clinopyroxenite zone (MCZ) and an upper gabbro zone (UGZ) (Fig. 3). The LOZ is composed of peridotitic cumulates with varying amounts of olivine, clinopyroxene and titanomagnetite (Fig. 4b). The MCZ consists mostly of clinopyroxenitic cumulates with the above cumulus assemblage and plagioclase appears in the upper part of this zone. The UGZ is composed of clinopyroxenitic and gabbroic cumulates with olivine, clinopyroxene, plagioclase and titanomagnetite as major minerals and apatite appears in the upper part of this zone. Six Fe–Ti oxide ore horizons, ranging from ~14 to 84 m in thickness, have been identified in the MCZ and UGZ (Zhong et al., 2002, 2005). According to the column section of Ma et al. (2003), however, the LOZ also contains Fe–Ti oxide ore horizons. During exploration in the 1970 s, various platinum-group minerals were found in the lower part of the intrusion and later work suggests that platinum-group element-rich horizons occur at the base of the LOZ and MCZ (Zhong et al., 2002).

3.3. Baima intrusion

The Baima intrusion (27°5′N, 102°6′E) covers an exposed area of over 50 km^2 and has thickness of over 1 km. The Baima Fe–Ti–(V) oxide deposit was discovered in 1955 by the geophysical team of the Sichuan Bureau of Geology (Ma et al., 2003) and large-scale mining operations started in 2008. The intrusion contains 1497 Mt of ore reserve with a mean grade of ~26% total Fe, ~7% TiO_2 and ~0.21% V_2O_5 (Ma et al., 2003). It was dated using the SHRIMP U–Pb zircon method at 261 ± 2 Ma and is divided from the base upwards into the Lower cumulate zone (LCZ), Oxide ore zone (OOZ), Olivine gabbro zone (OGZ) and Upper gabbro zone (UGZ) (Fig. 3). Igneous layering is generally west-dipping at shallow to medium angles. Oxide orebodies occur as conformable masses in the Oxide ore zone (up to ~70-m-thick) and, to a lesser extent, in the OGZ. The LCZ, OGZ and UGZ consist of gabbroic and oxide gabbroic cumulates with varying amounts of olivine, clinopyroxene, plagioclase and titanomagnetite. Cumulus apatite is restricted to the upper part of the OGZ. The OOZ is composed mainly of Fe–Ti oxide cumulates with titanomagnetite as the main cumulus mineral. Contemporaneous granitoids include peralkaline syenite to the southwest, the Woshui metaluminous syenite to the east, and the Cida granite to the northeast of the Baima intrusion (Shellnutt and Zhou, 2007; Shellnutt et al., 2009; Zhong et al., 2007).

3.4. Taihe intrusion

The Taihe intrusion (27°54′N, 102°7′E) covers an exposed area of ~13 km^2 and has thickness of over 1 km. Mining of the Taihe Fe-Ti-(V) oxide deposit began in 1988 but has been semi-stagnant due to the low ore grade compared to the other deposits. Its estimated ore reserve and mean ore grade are similar to the Panzhihua intrusion (Zhong et al., 2005). Unpublished laser-ablation inductively coupled plasma mass spectrometry U–Pb zircon geochronologic data by one of the authors (JGS) suggest a crystallization age of 264 ± 3 Ma. The ores occur over an interval of 400 to 700 m in the lower part of the intrusion. Faulting has severely affected the intrusion and destroyed its internal structure and continuity. The intrusion is cut by basaltic and syenitic dykes, ranging from <5 to 20 m in thickness, mostly along faults and joints. Granites to the west of the intrusion were dated at ~260 Ma (Luo et al., 2006). However, the fault between the intrusion and the granite as shown in local geological maps is not visible in the field.

3.5. Xinjie intrusion

The Xinjie intrusion (26°55′N, 102°8′E) is a 7.5-km-long and 1.2-km-thick mafic–ultramafic sill striking northwest. It contains Fe–Ti–(Cr) oxide and Ni–Cu–(PGE) sulfide mineralization. The intrusion is only exposed in several small outcrops, but was explored by drilling in the 1980s by a local geological team (PXGT, 1981). The intrusion was dated using the SHRIMP U–Pb zircon method at 259 ± 3 Ma (Zhou et al., 2002). It was emplaced into the Emeishan flood basalts and syenite is present at its hangingwall. The intrusion exhibits well-developed igneous layering and the layers dip at high angles to the southwest. The Xinjie intrusion is divided into the Marginal zone overlain by three cyclic units (I, II and III) (Fig. 3). The Marginal zone is composed of microgabbros and olivine microgabbros with partially-digested xenoliths of basalts. Each cyclic unit is more mafic towards its base and less mafic towards its top. Cycle I consists of peridotitic, clinopyroxenitic and gabbroic cumulates. Cycle II and III are composed mainly of clinopyroxenitic and gabbroic cumulates. Olivine, clinopyroxene, plagioclase, titanomagnetite, ilmenite and chrome spinel are major cumulus phases. Oxide ore horizons occur in the upper parts of cycle I and cycle II (Zhong et al., 2004).

4. Ore petrography

The petrography of Fe–Ti oxide ores in layered intrusions in the Panxi region has been described in detail by Zhou et al. (2005), Pang et al. (2008a) and Wang et al. (2008), and we only provide a brief summary here. Oxide ores range from semi-massive to massive with varying amounts of silicate minerals, which also occur in the gabbroic and pyroxenitic host rocks. Ore minerals include magnetite and ilmenite grains (mostly 1 to 1.5 mm), the boundaries of which are commonly marked by ~120° triple junctions. Such granoblastic texture is commonly suggested to have formed from mutual adjustment of grain boundaries in the solid state to achieve textural equilibrium (Reynolds, 1985; Hunter, 1987; Libourel and Krot, 2007). In domains containing more silicates, Fe–Ti oxides tend to have curved boundaries against the silicates and appear to be filling gaps between them (Fig. 4c and d). The amounts, types and distributions of silicate minerals occurring in the ores are variable, even on the scale of a thin section. Magnetite in the ores contains very fine blebs or lamellae of ulvöspinel and hercynitic spinel along its (100) planes. Much thicker lamellae of ilmenite are present in places in some grains. Ilmenite is generally free of micro-intergrowths, except in the Xinjie intrusion that part of it contains magnetite (hematite?) intergrowths. Reaction rims of hornblende or olivine are well-developed along some contacts between silicates and Fe–Ti oxides. In addition, base-metal sulfides and green spinel are common accessory minerals but their occurrences are sporadic. The ores are completely free of apatite.

5. Geochemical features of the ore-bearing intrusions

We compiled 229 major element, 205 trace element and 72 Sr–Nd isotopic analyses from seven geochemical studies on the Fe–Ti oxide ore-bearing layered intrusions in the Panxi region. The full dataset is provided as a digital supplement. Representative electron microprobe analyses of Fe–Ti oxides in the Hongge and Baima intrusions are given in Table 1.

The data show wide ranges of major element concentrations, especially SiO_2, TiO_2 and Fe_2O_3 that are attributable to accumulation of Fe–Ti oxides. The linear trends shown by most binary plots of major element against SiO_2 indicate mixing between Fe–Ti oxides and silicate phases (Fig. 5). The clustering of the Xinjie data most likely stems from the lack of available analyses of oxide-rich samples. The trends of Fe and Ti for the Panzhihua, Hongge, Baima and Taihe samples display negative slopes characteristic of the accumulation of Fe–Ti oxides. These trends for all intrusions, except Hongge, extrapolate at zero SiO_2 to ~14 to 16 wt.% TiO_2 and ~78 to 80 wt.% Fe_2O_3, reflecting titanomagnetite control. The trend for the Hongge samples extrapolates to ~22 wt.% TiO_2 and 62 wt.% Fe_2O_3, reflecting both titanomagnetite and ilmenite control. The Ca trends for these intrusions exhibit positive slopes extending to ~15 wt.% CaO, indicative of accumulation of Ca-rich pyroxene. The Al and total alkalis trends for the Panzhihua, Baima and Taihe samples also show positive slopes reflecting the accumulation of plagioclase. Some Panzhihua samples show a negatively-sloped P_2O_5 trend indicating the presence of cumulus apatite, but the P_2O_5 contents for the majority of samples in other intrusions do not exceed ~0.5 wt.%.

Minor elements V, Ni and Cr exhibit large ranges of absolute concentrations, chiefly attributable to controls by titanomagnetite, olivine and chrome spinel, respectively. Vanadium concentration ranges from some 100 ppm or lower in silicate rocks to ~4800 ppm in Fe–Ti oxide ores (Fig. 5). Ranges of Ni and Cr concentrations show greater variability in a given intrusion; samples from intrusions consisting of ultramafic parts (e.g. Hongge, Xinjie) contain some 1000 ppm or higher of these elements (see Supplementary data). Trace elements exhibit wide ranges of absolute concentrations. Concentrations of large-ion-lithophile elements, such as Rb and Ba, range from several ppm or lower to several hundred ppm. Concentrations of individual rare-earth elements (REE) range from 1 ppm or lower to several ppm even without cumulus apatite. Concentrations of high-field-strength elements (HFSE), such as Hf and Ta, range from 0.1 ppm or lower to several ppm. Since most of these elements are thought to behave incompatibly in minerals occurring in the ore-bearing intrusions, the variations are largely attributable to varying amounts of trapped liquids during cumulate formation. In primitive mantle-normalized spider diagrams, the patterns are similar to ocean island basalts characterized by general negative slopes (Fig. 6). Most of them display prominent negative Zr–Hf anomalies, which cannot be explained by mantle processes because these features are absent in the contemporaneous Emeishan flood basalts (Xu et al., 2001; Xiao et al., 2004). Instead, they can be accounted for by the presence of cumulus apatite that preferentially concentrates REE compared to HFSE. For example, a large number of Panzhihua samples, one Hongge sample and one Baima sample showing strong negative Zr–Hf anomalies have high REE (~10 to 100 × primitive mantle) and P_2O_5 concentrations (not shown). Some Xinjie samples display the strongest negative Y anomaly in the entire dataset that are probably due to analytical problems (see Supplementary data).

Fig. 7 shows the Sr–Nd isotopic compositions of the ore-bearing intrusions, corrected to an age of 260 Ma. The initial $^{87}Sr/^{86}Sr$ ratios and $\varepsilon Nd(t)$ of most samples range from 0.7043 to 0.7066 and from 0 to +4, respectively (Fig. 7). Exceptions include a Baima sample (GS04-135) characterized by high Rb concentration (~92 ppm), high $^{87}Rb/^{86}Sr$ ratio

Table 1
Compositions of magnetite–ilmenite pairs from the Hongge and Baima intrusions used for Fe–Ti oxide geothermobarometry.

Intrusion	Hongge																								
Sample	HGI-29		HGI-29		HGI-32		HGI-32		HGI-4		HGI-14		HGI-14		HGI-14		HGI-14		HGI-14		HGI-14		HGI-14		HGI-15
Rock[a]	Ore		Ore		Ore		Ore		Gb		Ol-cpx		Ol-cpx		Ol-cpx		Ol-cpx		Ol-cpx		Ol-cpx		Ol-cpx		Ol-cpx
Pair	#1		#2		#1		#2		#1		#1		#2		#3		#4		#5		#6		#7		#1
Mineral	Mt	Ilm	Mt	Ilm	Mt	Ilm	Mt	Ilm	Mt	Ilm	Mt	Ilm	Mt	Ilm	Mt	Ilm	Mt	Ilm	Mt	Ilm	Mt	Ilm	Mt	Ilm	Mt
n[b]	2	2	2	2	2	2	2	2	4	3	1	1	1	1	1	1	1	1	1	1	1	1	1	1	1
TiO_2	16.67	57.24	16.74	56.09	13.32	55.64	13.05	55.40	6.45	51.07	0.64	50.96	0.75	50.84	0.81	51.05	0.70	51.51	0.59	51.65	2.87	51.06	2.55	52.03	0.57
Al_2O_3	2.37	n.d.[c]	3.49	n.d.	2.45	n.d.	3.19	n.d.	2.25	n.d.	0.64	n.d.	0.28	n.d.	0.63	n.d.	0.35	n.d.	0.33	n.d.	2.30	n.d.	1.06	n.d.	0.27
Cr_2O_3	2.84	0.04	3.58	0.08	5.03	0.10	5.38	0.04	0.06	0.02	1.55	0.12	1.46	0.06	1.66	0.07	1.40	0.11	1.65	0.03	1.67	0.02	1.49	0.06	2.74
V_2O_3	n.d.	n.d.	n.d.	n.d.	n.d.	n.d.	n.d.	n.d.	n.d.	n.d.	0.85	0.15	0.85	0.37	0.83	0.38	0.91	0.36	0.88	0.33	0.83	0.27	0.73	0.22	1.02
Fe_2O3	34.81	1.72	31.38	3.60	36.86	2.22	36.37	1.63	53.75	7.24	65.58	2.39	66.15	2.39	65.67	2.40	65.76	2.42	65.71	2.42	58.91	2.40	61.96	2.44	65.19
FeO	39.16	30.14	39.79	29.28	38.44	33.52	38.29	34.45	35.93	36.73	31.43	43.00	31.52	41.03	31.33	41.29	30.88	39.30	30.93	41.35	32.40	40.56	33.12	40.07	31.09
MnO	0.30	0.30	0.36	0.39	0.43	0.46	0.34	0.47	0.08	0.57	0.00	0.88	0.00	0.68	0.00	0.63	0.00	0.44	0.08	0.66	0.04	0.77	0.00	0.86	0.00
MgO	5.01	11.76	4.54	11.63	3.10	8.97	3.36	8.34	0.75	4.80	0.23	1.76	0.27	3.32	0.50	3.57	0.49	4.61	0.35	2.88	0.91	3.00	0.44	3.97	0.42
Total	101.15	101.20	99.88	101.07	99.62	100.91	100.00	100.33	99.27	100.44	100.92	99.25	101.27	98.68	101.43	99.38	100.48	98.74	100.53	99.32	99.93	98.07	101.35	99.66	101.30
Ti	0.44	0.66	0.45	0.65	0.37	0.65	0.36	0.66	0.18	0.62	0.02	0.94	0.02	0.93	0.02	0.92	0.02	0.93	0.02	0.94	0.08	0.95	0.07	0.93	0.02
Al	0.10		0.15		0.11		0.14		0.10		0.03		0.01		0.03		0.02		0.01		0.10		0.05		0.01
Cr	0.08	0.00	0.10	0.00	0.15	0.00	0.15	0.00	0.00	0.00	0.05	0.00	0.04	0.00	0.05	0.00	0.04	0.00	0.05	0.00	0.05	0.00	0.04	0.00	0.08
V											0.03	0.00	0.03	0.01	0.03	0.01	0.03	0.01	0.03	0.01	0.02	0.01	0.02	0.00	0.03
Fe^{3+}	0.93	0.02	0.85	0.04	1.02	0.03	0.99	0.02	1.53	0.09	1.87	0.05	1.88	0.05	1.86	0.05	1.88	0.05	1.88	0.05	1.67	0.05	1.75	0.05	1.85
Fe^{2+}	1.16	0.38	1.19	0.37	1.18	0.44	1.16	0.45	1.14	0.50	1.00	0.92	1.00	0.88	0.99	0.88	0.98	0.84	0.99	0.88	1.02	0.87	1.04	0.85	0.98
Mn	0.01	0.00	0.01	0.01	0.01	0.01	0.01	0.01	0.00	0.01	0.00	0.02	0.00	0.01	0.00	0.01	0.00	0.01	0.00	0.01	0.00	0.02	0.00	0.02	0.00
Mg	0.26	0.27	0.24	0.27	0.17	0.21	0.18	0.20	0.04	0.12	0.01	0.06	0.02	0.12	0.03	0.13	0.03	0.16	0.02	0.10	0.05	0.11	0.02	0.14	0.02
Total	3.00	2.00	3.00	2.00	3.00	2.00	3.00	2.00	3.00	2.00	3.00	2.00	3.00	2.00	3.00	2.00	3.00	2.00	3.00	2.00	3.00	2.00	3.00	2.00	3.00

[a] Ore = Fe–Ti oxide ore, Gb = gabbro, Ol–cpx = olivine clinopyroxenite.
[b] n = number of analysis.
[c] n.d. = not determined.

											Baima													
	HGI-15		HGI-15		HGI-15		HGI-15		HGI-15		B-8		B-8		B-9		B-9		B-9		B-6		B-14	
	Ol-cpx		Ol-cpx		Ol-cpx		Ol-cpx		Ol-cpx		Ore		Ore		Ore		Ore		Ore		Gb		Gb	
	#2		#3		#4		#5		#6		#1		#2		#1		#2		#3		#1		#1	
Ilm	Mt	Ilm	Mt	Ilm	Mt	Ilm	Mt	Ilm	Mt	Ilm	Mt	Ilm	Mt	Ilm	Mt	Ilm	Mt	Ilm	Mt	Ilm	Mt	Ilm	Mt	Ilm
1	1	1	1	1	1	1	1	1	1	1	4	9	6	12	5	5	10	9	8	10	4	9	3	13
49.87	0.50	51.04	0.33	50.97	8.98	48.70	5.70	48.18	4.71	49.08	9.99	51.82	8.42	52.70	10.83	53.00	7.75	52.89	8.80	53.15	0.58	51.67	0.64	51.04
n.d.	0.35	n.d.	0.31	n.d.	2.23	n.d.	1.35	n.d.	1.01	n.d.	4.07	n.d.	1.74	n.d.	2.50	n.d.	2.66	n.d.	2.87	n.d.	0.58	n.d.	0.35	n.d.
0.07	3.26	0.09	2.66	0.17	0.13	0.05	0.15	0.12	0.15	0.05	0.19	0.03	0.18	0.01	0.10	0.01	0.13	0.01	0.13	0.01	0.12	0.01	0.12	0.01
0.20	0.82	0.21	0.84	0.23	0.84	0.15	0.74	0.33	0.71	0.21	n.d.	n.d.	n.d.	n.d.	n.d.	n.d.	n.d.	n.d.	n.d.	n.d.	n.d.	n.d.	n.d.	n.d.
2.34	64.88	2.40	65.76	2.39	48.89	2.29	54.78	2.26	56.44	2.30	44.51	3.66	50.46	2.68	45.15	1.99	50.83	2.19	48.28	1.73	67.09	2.25	67.52	4.97
43.58	31.36	40.61	31.02	41.94	38.86	44.26	33.10	44.11	33.85	44.04	37.22	39.26	37.16	39.87	39.35	41.97	36.58	41.00	37.29	41.20	31.62	45.00	31.78	41.35
0.53	0.00	0.44	0.00	0.75	0.40	0.62	0.24	0.68	0.10	0.76	0.39	0.79	0.29	0.82	0.38	1.03	0.35	0.86	0.39	0.93	0.04	1.33	0.04	1.37
3.22	0.29	4.46	0.35	3.36	0.29	2.84	1.44	2.97	0.39	2.76	1.84	3.66	0.94	3.73	1.04	2.60	1.02	3.16	1.11	3.15	0.02	0.05	0.03	1.77
99.81	101.45	99.23	101.26	99.81	100.62	98.90	97.50	98.66	97.35	99.20	98.20	99.23	99.19	99.82	99.34	100.59	99.32	100.12	98.87	100.17	100.04	100.31	100.47	100.51
0.90	0.01	0.92	0.01	0.92	0.25	0.90	0.17	0.89	0.14	0.90	0.28	0.64	0.24	0.65	0.31	0.65	0.22	0.65	0.25	0.66	0.02	0.65	0.02	0.64
	0.02		0.01		0.10		0.06		0.05		0.18		0.08		0.11		0.12		0.13		0.03		0.02	
0.00	0.10	0.00	0.08	0.00	0.00	0.00	0.00	0.00	0.00	0.00	0.01	0.00	0.01	0.00	0.00	0.00	0.00	0.00	0.00	0.00	0.00	0.00	0.00	0.00
0.00	0.02	0.00	0.03	0.00	0.03	0.00	0.02	0.01	0.02	0.00														
0.05	1.84	0.05	1.87	0.05	1.38	0.05	1.59	0.05	1.66	0.05	1.26	0.05	1.44	0.03	1.27	0.02	1.44	0.03	1.37	0.02	1.93	0.03	1.94	0.06
0.92	0.99	0.86	0.98	0.89	1.22	0.94	1.07	0.93	1.10	0.93	1.17	0.54	1.18	0.55	1.23	0.58	1.15	0.56	1.17	0.57	1.01	0.63	1.02	0.57
0.01	0.00	0.01	0.00	0.02	0.01	0.01	0.01	0.01	0.00	0.02	0.01	0.01	0.01	0.01	0.01	0.01	0.01	0.01	0.01	0.01	0.00	0.02	0.00	0.02
0.12	0.02	0.16	0.02	0.12	0.02	0.10	0.08	0.11	0.02	0.10	0.10	0.09	0.05	0.09	0.06	0.06	0.06	0.08	0.06	0.08	0.00	0.00	0.00	0.04
2.00	3.00	2.00	3.00	2.00	3.00	2.00	3.00	2.00	3.00	2.00	3.00	2.00	3.00	2.00	3.00	2.00	3.00	2.00	3.00	2.00	3.00	2.00	3.00	2.00

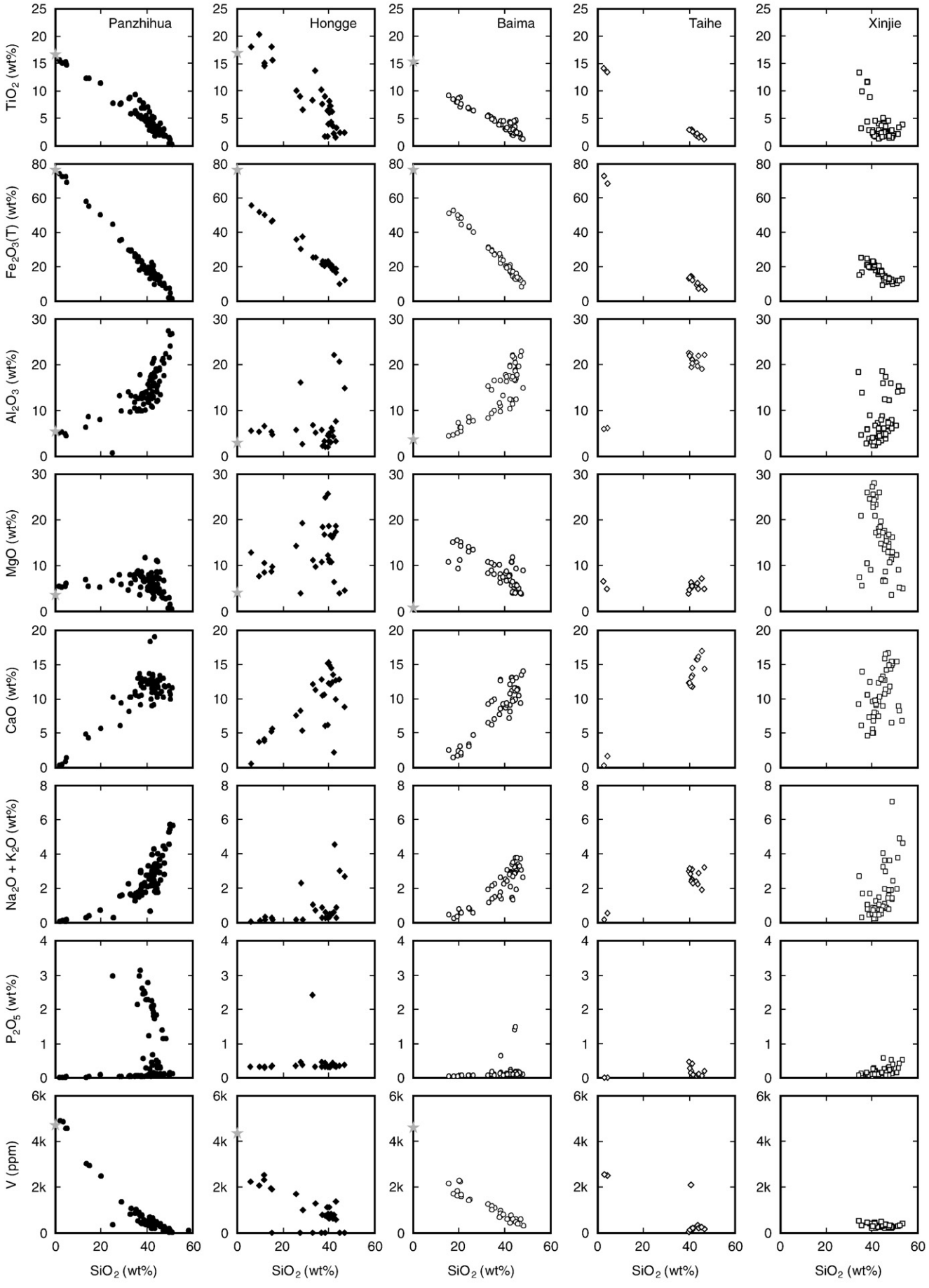
Panzhihua
Hongge
Baima
Taihe
Xinjie
TiO2 (wt%)
Fe2O3(T) (wt%)
Al2O3 (wt%)
MgO (wt%)
CaO (wt%)
Na2O + K2O (wt%)
P2O5 (wt%)
V (ppm)
SiO2 (wt%)

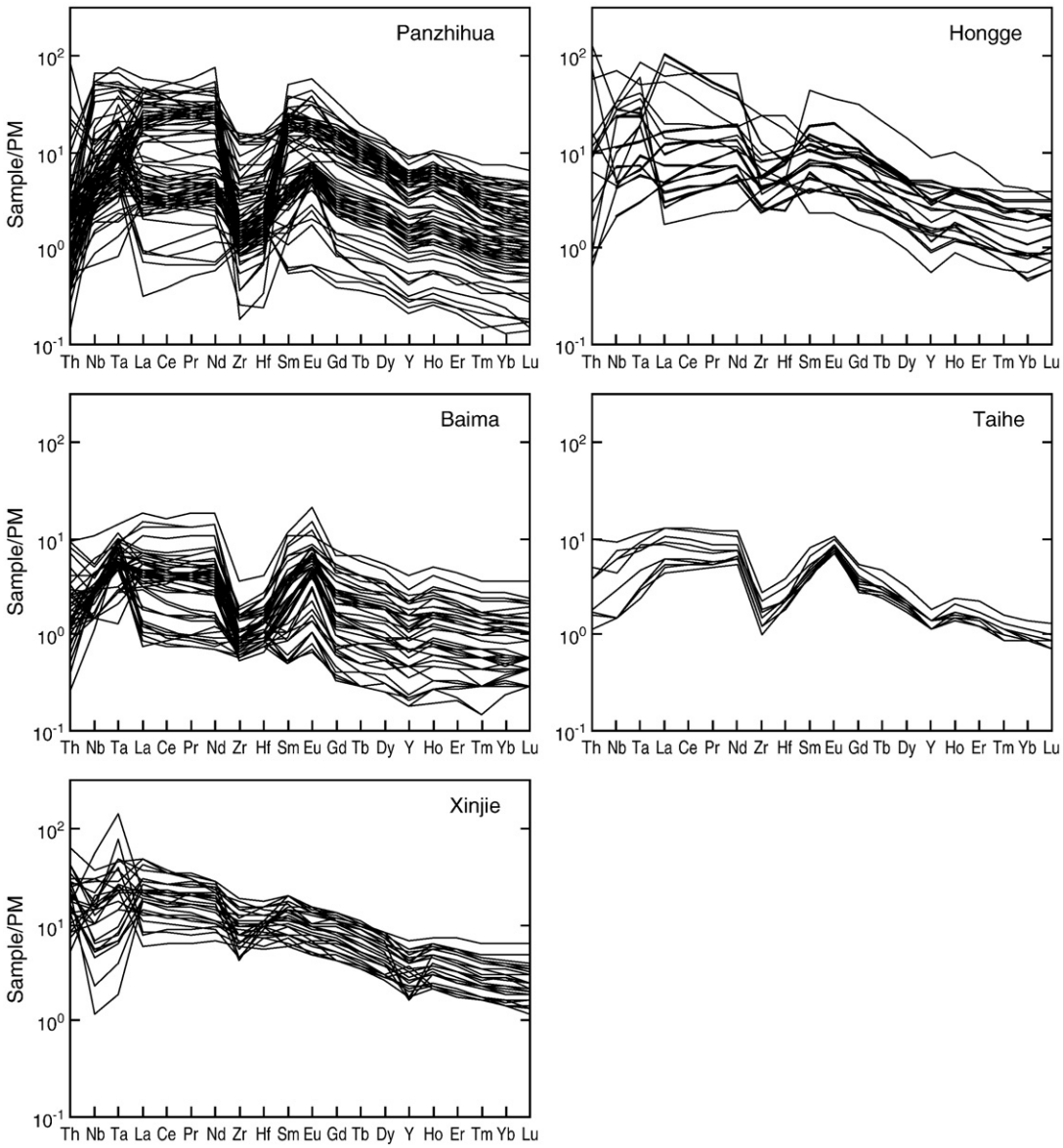

Fig. 6. Primitive mantle (PM)-normalized incompatible trace element patterns of the ore-bearing intrusions. Normalizing values after McDonough and Sun (1995).

(~16) and low initial $^{87}Sr/^{86}Sr$ ratio (0.703467) relative to other Baima samples. Another exception is a Panzhihua sample (PZH-28) that has low $^{143}Nd/^{144}Nd$ (0.512451) and hence low $\varepsilon Nd(t)$ (−2.14) than other Panzhihua samples. The majority of data plot in the field of high-Ti Emeishan basalts (Fig. 7).

6. Discussion

6.1. Comparison to other magmatic Fe–Ti oxide deposits

Table 2 lists the major characteristics of global magmatic Fe–Ti oxide deposits. Anorthosite-related deposits are associated with Proterozoic anorthosite complexes; examples include the Lac Tio deposit (Canada) and the Tellnes deposit (Norway) — the world's second largest ilmenite deposit (Lister, 1966; Duchesne, 1999). Oxide ores, dominated by either hemo-ilmenite or titanomagnetite and in many circumstances with apatite (the term *nelsonite* denotes Fe–Ti oxide-apatite rocks), occur as cross-cutting bodies in anorthosite, and to a lesser extent, leuconorite, leucogabbro and leucotroctolite (Table 2). The ores are commonly related to ferrodioritic (or jotunitic) parental magmas (Table 3) (Ashwal, 1993).

The second major type of Fe–Ti oxide deposits is hosted in upper parts of large layered intrusions; examples include the Bushveld Complex (South Africa) and the Windimurra Complex (Australia) (Lee, 1996). Oxide ores occur as layers, several tens of centimeters- to several meters-thick, characterized by great lateral continuity. In addition, the ores are associated with gabbronoritic, ferrogabbronoritic and ferrodioritic cumulates and have titanomagnetite as the dominant oxide mineral. Nelsonite may be present apart from pure titanomagnetite ores. The ores are suggested to crystallize and concentrate from an evolved magma of a basaltic parent after formation of extensive cumulates in the lower parts of the intrusions. Using the Bushveld Complex as an example, however, the evolved magma is not necessarily rich in TiO_2 (Table 3).

Fig. 5. Concentrations of major and minor element oxides of the ore-bearing layered intrusions. Sources: Hu et al. (2001), Zhong et al. (2002), Zhong et al. (2004), Zhou et al. (2005), Zhou et al. (2008), Shellnutt et al. (2009) and Zhang et al. (2009). The Taihe data are unpublished data by one of the authors (JGS). Grey stars denote reconstructed titanomagnetite composition (Panzhihua) (Pang et al., 2008a) or the most Ti-rich magnetite found in the intrusions (Hongge, Baima) (Ma et al., 2003; this study).

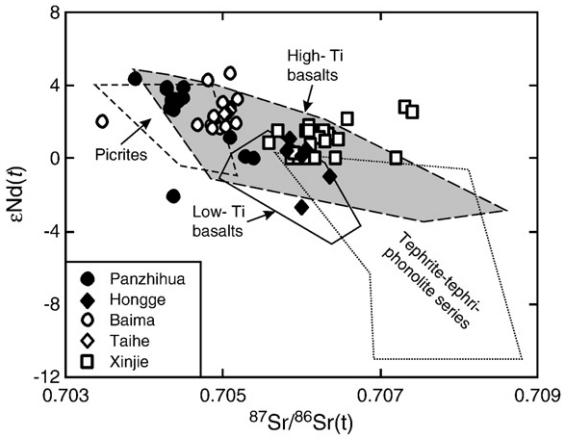

Fig. 7. Whole-rock initial εNd(t) versus initial $^{87}Sr/^{86}Sr$ ratios of the ore-bearing intrusions, calculated as $t = 260$ Ma. Different fields denote Sr–Nd isotopic compositions of volcanic rocks in the Emeishan LIP after Chung and Jahn (1995), Xu et al. (2001), Xiao et al. (2004), Zhang et al. (2006), Wang et al. (2007), Qi and Zhou (2008), Qi et al. (2008), Song et al. (2008).

The flood basalt-related Fe–Ti oxide deposits in the Panxi region possess some features exhibited by both types of deposits mentioned above (Table 2). However, they also display a number of distinctive features including (i) occurrences in a LIP, (ii) spatial and temporal association with considerable volumes of granitoids, (iii) formation from magmas rich in TiO_2 (see later discussions), (iv) occurrences of ores in low stratigraphic positions, (v) occurrences of ultramafic cumulates, in addition to gabbros, as host rocks, (vi) absence of apatite in ores hence nelsonite-free. For this reason, we propose that the flood basalt-related Fe–Ti oxide deposits in the Panxi region represent another major type of magmatic Fe–Ti oxide deposits.

6.2. Fe- and Ti-rich basaltic parental magmas

The Fe–Ti oxide ore-bearing intrusions in the Panxi region have been related genetically to high-Ti flood basalts of the Emeishan LIP (Zhong et al., 2005; Pang et al., 2008a; Zhou et al., 2008; Zhang et al., 2009). This is also evident by comparisons of Sr–Nd isotopes and Gd/Yb ratios between the intrusions and the basalts (see Figs. 7 and 8 for details), and we have no attempt to reiterate ideas already made by previous workers. However, earlier studies on the high-Ti basalts reveal appreciable compositional variability (MgO = 2.3–11.3 wt.%) that needs to be taken into account in examining possible parental magmas for the intrusions.

Pang et al. (2009) showed, on the basis of olivine-liquid Fe–Mg exchange equilibrium, that the Mg# [defined as molar $100 \times Mg/(Mg + Fe^{2+})$] of the parental magma of the Panzhihua intrusion ranges between 51 and 56. Similarly, Wang et al. (2008) showed that the parental magma of the Xinjie intrusion had molar Mg/Fe ratio of 0.88 (equivalent to Mg# of ~47). The most Mg-rich cumulus olivine documented from the Hongge and Baima intrusions is Fo_{84} and Fo_{76}, respectively (Ma et al., 2003). Assuming an olivine-liquid Fe–Mg

Table 2
Major characteristics of magmatic Fe–Ti oxide deposits worldwide.

Association	Host rock	Ore occurrence	Ore mineralogy[a]	Parental magma	Example
Proterozoic anorthosite complexes	Anorthosite, leuconorite, leucogabbro, leucotroctolite	Cross-cutting, massive lenses with sharp contacts against host rocks	Hemo-ilmenite or titanomagnetite, with or without apatite	Ferrodiorite[b]	Tellnes (Norway), Lac Tio (Canada)
Upper parts of large layered complexes	Gabbronorite, ferrogabbronorite, ferrodiorite	Conformable, laterally extensive layers with either sharp or gradational contacts against host rocks	Titanomagnetite, with or without apatite	Evolved, Fe-rich tholeiite	Bushveld (South Africa), Windimurra (Australia)
Lower parts of sub-volcanic intrusions associated with flood basalts	Gabbro, ferrogabbro, ultramafic cumulates	Conformable, massive lenses or layers with either sharp or gradational contacts against host rocks	Titanomagnetite, with or without ilmenite	High-Ti ferrobasalt	Panzhihua (China), Hongge (China)

[a] Only primary ore minerals are listed.
[b] The term jotunite has also been used to denote the same type of magma.

Table 3
Bulk compositions related to magmatic Fe–Ti oxide deposits.

	Fe-rich tholeiite	Ferrodiorite	Picrite	High-Ti basalts		
	(1)	(2)	(3)	(4)	(5)	(6)
SiO_2	49.79	49.78	44.47	46.89	43.93	44.86
TiO_2	0.82	3.02	2.35	3.30	3.12	3.61
Al_2O_3	15.82	14.37	11.15	10.13	14.80	11.08
Fe_2O_3	1.18	2.88	1.33	1.37	1.53	1.47
FeO	11.83	13.11	12.03	12.33	13.77	13.23
MnO	0.19	0.23	0.19	0.20	0.20	0.20
MgO	6.14	3.39	14.78	10.96	7.20	8.92
CaO	10.93	7.99	11.38	10.97	10.67	9.55
Na_2O	2.97	3.29	1.89	1.44	2.24	2.55
K_2O	0.25	1.20	0.08	1.98	1.21	1.22
P_2O_5	0.07	0.74	0.34	0.43	0.33	0.52
Mg#[b]	48	32	69	61	48	55

[a] Major and minor element oxides are in weight percent and are calculated to 100% total on a volatile-free basis.
[b] Mg# = [molar $100 \times Mg/(Mg + Fe^{2+})$], assuming 10% of total iron oxide is ferric.
(1) Proposed parental magma to Upper Zone, Bushveld Complex (Davies and Cawthorn, 1984).
(2) Average of 17 ferrodiorites, Harp Lake massif, Labrador (Ashwal, 1993).
(3) Picrite (sample DJ-2), Lijiang area, ELIP (Zhang et al., 2006).
(4) High-Ti basalt (sample LZS-41), Longzhoushan area, Emeishan LIP (Qi et al., 2008).
(5) High-Ti basalt (sample EM-78), Binchuan area, Emeishan LIP (Xu et al., 2001).
(6) High-Ti basalt (sample LZS-40), Longzhoushan area, Emeishan LIP (Qi et al., 2008).

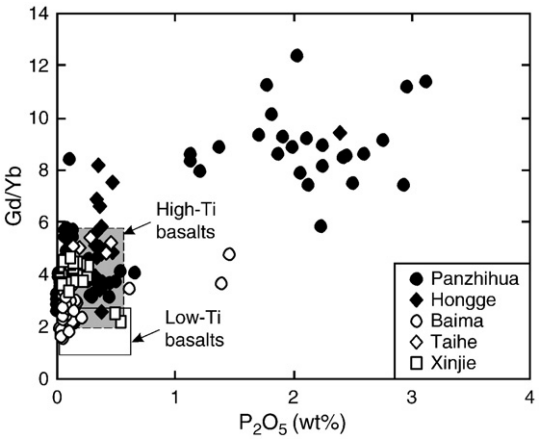

Fig. 8. Whole-rock Gd/Yb ratios versus P_2O_5 concentrations of the ore-bearing intrusions. Most samples with elevated Gd/Yb ratios (~6 or higher) also have high P_2O_5 concentrations (~1.2 wt.% or higher), indicating control by cumulus apatite, which preferentially concentrates middle REE. The rest majority of samples have Gd/Yb ratios consistent with high-Ti Emeishan basalts. The fields of Emeishan flood basalts after references listed in Fig. 7.

exchange coefficient (K_D) of 0.3 ± 0.03 (Roeder and Emslie, 1970), the equation

$$K_D = (FeO/MgO)_{olivine}/(FeO/MgO)_{melt}$$

yields Mg# of parental magmas of 61 (Hongge) and 48 (Baima). Combined with results for the Panzhihua and Xinjie intrusions, these compositions correspond to slightly- to moderately-fractionated high-Ti flood basalts (MgO = 7.2–11 wt.%) in the Emeishan LIP (Table 3). Olivine with Fo_{88} composition in the Xinjie intrusion (e.g. Zhong et al., 2004) probably has xenocrystic origin.

6.3. Early crystallization of Fe–Ti oxides

Several independent lines of evidence for early crystallization of Fe–Ti oxide include: (i) the occurrence of Fe–Ti oxide inclusions in relatively Mg-rich cumulus olivine (Fo_{78-81}) in the Panzhihua and Hongge intrusions (Pang et al., 2008b), (ii) relatively primitive silicate mineral compositions (i.e. high Fo of olivine, Mg# of clinopyroxene and An% of plagioclase) within or adjacent to Fe–Ti oxide ore horizons (Pang et al., 2009), and (iii) the occurrence of rare Ti-bearing chrome spinel and Cr-bearing titanomagnetite suggested to be early crystallizing phases in the Xinjie intrusion (Wang et al., 2008). Our compiled geochemical data are also consistent with these interpretations. First, the vast majority of cumulates in the Panzhihua, Hongge and Baima intrusions have TiO_2 concentrations higher than the parental magma compositions estimated in the above section (Fig. 5), which must indicate the presence of cumulus Fe–Ti oxides. Second, most cumulates in the Xinjie intrusion have moderate TiO_2 and high Fe_2O_3 concentrations (corrected from FeO analyses by wet chemistry) (Fig. 5), attributable to cumulus titanomagnetite. The lack of thick TiO_2-poor cumulates in the lower parts of these intrusions can be taken as evidence that liquidus Fe–Ti oxides started to crystallize before emplacement.

Wang et al. (2008) suggested that Fe–Ti-(Cr) oxides crystallized early in magma containing abundant Cr, a compatible element during evolution of mafic magmas. In fact, Cr-bearing titanomagnetite also occurs in some ore-bearing intrusions other than Xinjie. For example, Pang et al. (2008b) documented abundant Fe–Ti oxide inclusions in olivine (Fo_{78-81}) from the Panzhihua and Hongge intrusions and suggested that they are evidence of early Fe–Ti oxide crystallization. In their dataset, magnetite in the inclusions, composed of magnetite only or magnetite + ilmenite, contains 1.2 to 10.7 wt.% Cr_2O_3. In addition, our present data show that titanomagnetite in two Fe–Ti oxide ore samples of the Hongge intrusion contains 2.8 to 5.4 wt.% Cr_2O_3 (Table 1). The fact that the majority of ore-forming titanomagnetite is Cr-poor (~200 to 400 ppm) indicates that enrichment in Cr may be characteristic of the first liquidus magnetite. Given the density relations of Fe–Ti oxides and other silicate phases in basaltic systems (see Scoates, 2000), gravitational accumulation of early-crystallized, liquidus Fe–Ti oxides provides the best explanation for ore occurrences to date.

6.4. Intensive parameters

6.4.1. Pressure

The spatial and temporal associations between the Fe–Ti oxide ore-bearing layered intrusions and flood basalts of the Emeishan LIP indicate that the intrusions likely represent sub-volcanic magmatic systems. The Xinjie intrusion was emplaced into the basalts lying along its lower contact, whereas the Hongge intrusion was emplaced into the base of the flood basalts (Fig. 3). Contemporaneous granitoids associated with the Panzhihua and Taihe intrusions, interpreted to be residual liquids, intruded the flood basalts, suggesting that the intrusions were also emplaced at relatively shallow levels. The Baima intrusion was probably emplaced in a similar manner as Panzhihua and Taihe, although the strong deformation associated with it obscures the field relations. Therefore, the ore-bearing intrusions likely crystallized at low pressure in the following order of decreasing depth of emplacement: Panzhihua, Baima, Taihe > Hongge > Xinjie.

Pang et al. (2008a) estimated the primary oxide composition in the Panzhihua intrusion to be an aluminous titanomagnetite with ~5.3 wt.% Al_2O_3 in solid solution, suggesting that it crystallized at a pressure of 3 to 5 kbar as elevated pressure generally favours the $MgAl_2O_4$ component and its incorporation into spinel. The Al_2O_3 versus SiO_2 diagrams indicate that this is also valid for other ore-bearing intrusions except the Xinjie intrusion (Fig. 5). They exhibit trends extrapolating at zero SiO_2 to ~5 wt.% Al_2O_3 (Hongge, Baima), and/or have data plotted close to that value at low SiO_2 concentrations (Taihe). This feature, together with independent electron microprobe data on Fe–Ti oxides (also plotted in Fig. 5), suggest that the primary titanomagnetite in the Hongge, Baima and Taihe intrusions contains appreciable quantities of Al_2O_3 as in the Panzhihua intrusion. Assuming that lithostatic pressure is largely contributed by flood basalts overlying the intrusions, the pressure range of 3–5 kbar mentioned above corresponds to 10 to 17 km of basalts (average density = 3.0 g cm^{-3}), a thickness far exceeding the thickest (~5 km) volcanic succession preserved in the Emeishan LIP. It thus seems more likely that the intrusions formed by emplacement of magmas containing titanomagnetite that had started to crystallize at depth.

6.4.2. Oxygen fugacity

Extensive subsolidus re-equilibration and exsolution typical of Fe–Ti oxides in plutonic rocks commonly overprint any high-temperature information that can be retrieved by Fe–Ti oxide geothermobarometry (Buddington and Lindsley, 1964; Frost et al., 1988). For this reason, Pang et al. (2008a) and Wang et al. (2008) failed to obtain magmatic temperatures and oxygen fugacity when applying this method to the Panzhihua and Xinjie intrusions, respectively. Not surprisingly, the Baima and Hongge data in this study also reveal subsolidus temperatures and their corresponding values of oxygen fugacity cannot be simply extrapolated to higher magmatic temperatures (Fig. 9).

Pang et al. (2008a) obtained titanomagnetite composition of ~40 mol% ulvöspinel (Usp_{40}) after careful reconstruction from microprobe analyses and showed that it is the only oxide mineral accumulated in the ores. These authors also demonstrated that this mineral last equilibrated with olivine and clinopyroxene at ~950 °C

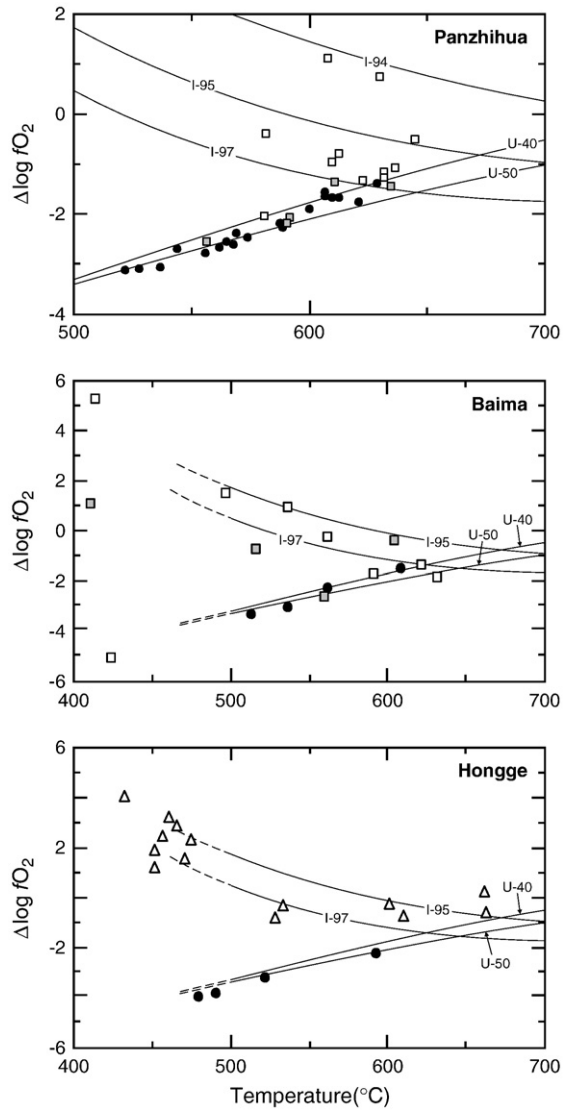

Fig. 9. Relations between oxygen fugacity and temperature calculated from coexisting magnetite and ilmenite by the QUILF program (Andersen et al., 1993). Oxygen fugacity is normalized to that of the fayalite–magnetite–quartz (FMQ) buffer, where log fO_2 (ΔFMQ) = log fO_2 − log fO_2 (FMQ). Lines labeled "I" or "U" is isopleths of ilmenite and ulvöspinel, respectively, adapted from Frost et al. (1988). Filled circles = Fe–Ti oxide ores, filled squares = oxide gabbro, empty squares = gabbro, triangle = clinopyroxenite. Mineral pairs in silicate rocks plot on or close to the ilmenite isopleths (Ilm_{95-97}), indicating that these rocks contain ilmenite as the dominant Fe–Ti oxides, either primary in origin or formed by complete oxidation of titanomagnetite. In contrast, mineral pairs in Fe–Ti oxide ores follow tightly the ulvöspinel isopleths (Usp_{40-50}), suggesting that they are composed dominantly of titanomagnetite as observed in the Panzhihua intrusion (Pang et al., 2008a).

and oxygen fugacity between FMQ + 1 to FMQ + 1.5 by intersecting the Usp_{40} isopleth with a olivine–clinopyroxene–Usp_{40} surface calculated using QUILF. In their dataset, many of the (un-reconstructed) magnetite–ilmenite pairs in the ores plot close to the Usp_{40} isopleth (Fig. 9), consistent with the primary oxide being dominated by Usp_{40} titanomagnetite. We draw attention to the Baima and Hongge ores that also plot close to the Usp_{40} isopleth (Fig. 9). If the ore-forming primary oxides in these intrusions have ~Usp_{40} composition, then it is possible that oxide-silicate equilibration ceased at ~950 °C and oxygen fugacity between FMQ + 1 to FMQ + 1.5 as in the Panzhihua intrusion.

Melting experiments in ferrobasalts demonstrate that the partitioning of V in magnetite is a function of oxygen fugacity (Toplis and Corgne, 2002 and references therein). Vanadium exists as V^{3+}, V^{4+} and V^{5+} in basaltic magmas and the magnetite–melt partition coefficient for V^{3+} is much greater than V^{4+} and V^{5+}. Magnetite crystallized under reducing condition is richer in V compared to that crystallized under oxidizing condition due to changing $V^{3+}/\Sigma V$ ratio in magmas. This relation is exemplified by various natural occurrences including the V-poor titanomagnetite in the Suwalki massif-type anorthosite (Poland) (0.2 to 0.67 wt.%V, FMQ + 2 to FMQ + 3.5) (Charlier et al., 2009), and the V-rich, first liquidus titanomagnetite in the Bushveld Complex (~1.3 wt.%V, NNO − 1.5 to NNO, equivalent to FMQ − 2.6 to FMQ − 1.1, Frost, 1991) (Cawthorn and Molyneux, 1986; Toplis and Corgne, 2002) and in the Fedorivka layered intrusion (Ukraine) (~1.85 wt.%V, FMQ − 1.4 to FMQ + 0.7) (Duchesne et al., 2006). The low V concentration (<4800 ppm) of magnetite from Fe–Ti oxide deposits in the Panxi region (Fig. 5) is consistent with formation under relatively high oxygen fugacity. Experimental data in P-free systems by Toplis and Corgne (2002) indicate a linear trend between magnetite–melt V partitioning and oxygen fugacity that can be expressed by the equation

$$V_{magnetite}/V_{magma} = -9.39(\Delta FMQ) + 37.45$$

where $V_{magnetite}$ and V_{magma} are concentrations of V in magnetite and in magma, respectively, and ΔFMQ is the oxygen fugacity expressed in terms of log units relative to the fayalite–magnetite–quartz (FMQ) buffer. If V_{magma} is fixed at 300 ppm, a value similar to the average V concentration of high-Ti basalts having Mg# = 54 to 60 (n = 18; Qi et al., 2008), the V concentration of cumulus titanomagnetite (4400 to 4800 ppm V) in the intrusions yields oxygen fugacity of FMQ + 2.3 to FMQ + 2.4.

The oxygen fugacity estimated using V in magnetite is higher than inferred from Fe–Ti oxide-silicate equilibria. One possible explanation is that oxygen fugacity evolved from higher values during titanomagnetite crystallization to lower values at which oxide and silicate minerals ceased to equilibrate. Nevertheless, it is clear that both approaches yield elevated oxygen fugacity relative to the majority of basaltic magmas (Ballhaus, 1993; Mallmann and O'Neill, 2009). Ganino et al. (2008) suggested that the release of CO_2 from carbonate country rocks in the Panzhihua intrusion would have raised the oxygen fugacity of the magma and triggered crystallization of abundant magnetite. However, most other ore-bearing intrusions in the region were not emplaced into carbonate rocks and the wide applicability of this model remains uncertain (Fig. 3). Alternatively, elevated oxygen fugacity might be an inherited feature of an oxidized mantle source from which the parental magmas of the intrusions originated or interacted (Brandon and Draper, 1996; Blatter and Carmichael, 1998).

6.5. Implications for mineral exploration

Magmatic Fe–Ti oxide deposits have not been documented in other well-studied LIPs aside from the Emeishan LIP. There are two possible explanations. First, the well-studied LIPs are characterized by thick successions of continental flood basalts in the order of several hundred meters to several kilometers (e.g. MacDougall, 1988) and the underlying ore-bearing intrusions remain largely unexposed. Second, ore formation probably requires very specific factors, either chemical (e.g. mantle source and parental magma compositions, oxygen fugacity) or physical (e.g. magma chamber dynamics, plumbing systems), that are only present in some LIPs. Among them, we draw attention to the issue of oxygen fugacity discussed above. If magma-carbonate rock interaction is the key to raise oxygen fugacity in magma and to trigger ore formation (Ganino et al., 2008), then this type of deposits is more likely to be found in LIPs that are emplaced into sedimentary basins in which carbonate strata are abundant.

Flood basalt-related Fe–Ti oxide deposits or mineralization are probably far more than common and we provide certain potential examples. The ~564 Ma Sept Iles intrusion (Canada) is contemporaneous with widespread basaltic and alkaline magmatism in eastern Laurentia (Higgins, 2005; Namur et al., 2010). The intrusion is suggested to undergo early Fe–Ti oxide crystallization that formed 24 layers of Fe–Ti oxides up to 1 m-thick. Within the ~1.1 Ga Mid-continent Rift (Keweenawan LIP), a number of Fe–Ti oxide-rich intrusions of the Duluth Complex are described as "oxide-rich ultramafic intrusions" and are relatively poor in apatite (Severson, 1988; Ripley et al., 1998). The ~1.2 Ga Smålands Taberg Fe–Ti oxide deposit (Sweden) is contemporaneous with a widespread magmatic event dominated by mafic dike swarms and granitoids (Larsson and Söderlund, 2005). Uniform olivine (Fo_{70}) and plagioclase (An_{53}) compositions in the ores documented by Sandecki (2000) also point to early Fe–Ti oxide crystallization.

7. Conclusions

This study of magmatic Fe–Ti oxide deposits in the Panxi region, Emeishan LIP (SW China) provides constraints on the formation of oxide ores and their hosting layered intrusions. The ore-bearing intrusions formed from parental magmas similar to the slightly- to moderately-fractionated high-Ti Emeishan flood basalts (MgO = 7.2–11 wt.%) that were emplaced in sub-volcanic environments. Whole-rock geochemical data indicate that large amounts of cumulus Fe–Ti oxides (titanomagnetite ± ilmente) are present throughout the intrusions, consistent with early Fe–Ti oxide crystallization following magma emplacement as previously proposed. Rare Cr-bearing titanomagnetite in the Panzhihua, Hongge and Xinjie intrusions is suggested to be characteristic of the first liquidus titanomagnetite. Crystallization under relatively high oxygen fugacity resulted in V-poor (<4800 ppm) titanomagnetite. Comparison between the flood basalt-related Fe–Ti oxide deposits and anorthosite-related deposits or those hosted in upper parts of large layered intrusions reveals substantial differences in terms of host rocks, ore occurrences, ore mineralogy, parental magmas, and the aforementioned ore-forming processes and conditions. The flood basalt-related oxide deposits in the Panxi region represent a new type of magmatic Fe–Ti oxide deposits that are potential exploration targets in other continental flood basalt provinces.

Acknowledgements

We thank Yuxiao Ma and Jun-Hong Zhao for assistance in the 2004 field excursion. Comments by guest editor Sun-Lin Chung, overseeing editor Nelson Eby and reviewers Bernard Charlier and James Scoates markedly improved the quality of the paper. Logistic support by Panzhihua Steel Co. Ltd. is gratefully acknowledged. This work is partially supported by a Chinese 973 project (2007CB411401) to MFZ and CAS/SAFEA International Partnership Program for Creative Research Teams (KZCX2-YW-t004). Additional support was obtained from a "CAS Hundred Talents" Project from Chinese Academy of Sciences (KZCX2-YW-BR-09) to LQ.

Appendix A. Analytical methods

Mineral compositions of Fe–Ti oxides from the Hongge and Baima intrusions were determined using a Cameca SX50 electron microprobe at The University of South Carolina, U.S.A. Samples from the Hongge intrusion were collected from abandoned open-cast mine workings and those from the Baima intrusion were collected from drillcore and analyzed for major and trace elements by Zhou et al. (2008). Selected areas of magnetite grains with the finest possible exsolution micro-intergrowths were analyzed. In case no single area can be found, analyses were performed on different parts of a given magnetite grain and an average composition was obtained. Analytical conditions and standards were identical to those described in Pang et al. (2008a). Repeat analyses of optically homogeneous titanomagnetite grains and laboratory standards suggest that the precision is better than ±2% (relative) for most elements.

Appendix B. Supplementary data

Supplementary data associated with this article can be found, in the online version, at doi:10.1016/j.lithos.2010.06.003.

References

Andersen, D.J., Lindsley, D.H., Davidson, P.M., 1993. QUILF: a Pascal program to assess equilibria among Fe–Mg–Mn–Ti oxides, pyroxene, olivine, and quartz. Computers and Geosciences 19, 1333–1350.
Ali, J.R., Thompson, G.M., Song, X., Wang, Y., 2002. Emeishan basalts (SW China) and the "end-Guadalupian" crisis: magnetobiostratigraphic constraints. Journal of the Geological Society 159, 21–29.
Ali, J.R., Thompson, G.M., Zhou, M.-F., Song, X., 2005. Emeishan large igneous province, SW China. Lithos 79, 475–489.
Ashwal, L.D., 1993. Anorthosites. Springer-Verlag, Berlin, Heidelberg, p. 148.
Ballhaus, C., 1993. Redox states of lithospheric and asthenospheric upper mantle. Contributions to Mineralogy and Petrology 114, 331–348.
Blatter, D.L., Carmichael, I.S.E., 1998. Hornblende peridotite xenoliths from central Mexico reveal the highly oxidized nature of subarc upper mantle. Geology 26, 1035–1038.
Brandon, A.D., Draper, D.S., 1996. Constraints on the origin of the oxidation state of mantle overlying subduction zones: an example from Simcoe, Washington, USA. Geochimica et Cosmochimica Acta 60, 1739–1749.
Buddington, A.F., Lindsley, D.H., 1964. Iron–titanium oxide minerals and synthetic equivalents. Journal of Petrology 5, 310–357.
Cawthorn, R.G., Molyneux, T.G., 1986. Vanadiferous magnetite deposits of the Bushveld Complex. In: Anhaeusset, C.R., Maske, S. (Eds.), Mineral Deposits of Southern Africa. Geol. Soc. S. Africa, Johannesburg, pp. 1251–1266.
Charlier, B., Namur, O., Duchesne, J.-C., Wiszniewska, J., Parecki, A., Vander Auwera, J., 2009. Cumulate origin and polybaric crystallization of Fe–Ti oxide ores in the Suwalki Anorthosite, northeastern Poland. Economic Geology 104, 205–221.
Chung, S.-L., Jahn, B.-M., 1995. Plume–lithosphere interaction in generation of the Emeishan flood basalts at the Permian–Triassic boundary. Geology 23, 889–892.
Davies, G., Cawthorn, R.G., 1984. Mineralogical data on a multiple intrusion in the Rustenburg Layered Suite of the Bushveld Complex. Mineralogical Magazine 48, 469–480.
Duchesne, J.C., 1999. Fe–Ti deposits in Rogaland anorthosites (South Norway): geochemical characteristics and problems of interpretation. Mineralium Deposita 34, 182–198.
Duchesne, J.C., Shumlyanskyy, L., Charlier, B., 2006. The Fedorivka layered intrusion (Korosten Pluton, Ukraine): an example of highly differentiated ferrobasaltic evolution. Lithos 89, 353–376.
Force, E.R., 1991. Geology of titanium mineral deposits. Geological Society of America Special Paper 259, 1–112.
Frost, B.R., 1991. Introduction to oxygen fugacity and its petrologic importance. In: Lindsley, D.H. (Ed.), Oxide Minerals: Petrologic and Magnetic Significance. Reviews in Mineralogy, 25. Mineralogical Society of America, Washington, pp. 1–9.
Frost, B.R., Lindsley, D.H., Andersen, D.J., 1988. Fe–Ti oxide-silicate equilibria: assemblages with fayalitic olivine. American Mineralogist 73, 727–740.
Ganino, C., Arndt, N.T., Zhou, M.-F., Gaillard, F., Chauvel, C., 2008. Interaction of magma with sedimentary wall rock and magnetite ore genesis in the Panzhihua mafic intrusion, SW China. Mineralium Deposita 43, 677–694.
Higgins, M.D., 2005. A new interpretation of the structure of the Sept Iles Intrusive suite, Canada. Lithos 83, 199–213.
Hu, S.-F., Zhong, H., Liu, B.-G., Zhou, X.-H., 2001. Geochemistry of the Hongge layered intrusion in the Panxi area. Geochemica 30, 131–139 (in Chinese).
Hunter, R.H., 1987. Textural equilibrium in layered igneous rocks. In: Parsons, I. (Ed.), Origins of Igneous Layering. D. Reidel Publishing Company, pp. 473–503.
Irvine, T.N., 1982. Terminology for layered intrusions. Journal of Petrology 23, 127–162.
Larsson, D., Söderlund, U., 2005. Lu–Hf apatite geochronology of mafic cumulates: an example from a Fe–Ti mineralization at Smålands Taberg, southern Sweden. Chemical Geology 224, 201–211.
Lee, C.A., 1996. A review of mineralization in the Bushveld Complex and some other layered intrusions. In: Cawthorn, R.G. (Ed.), Layered Intrusions. Amsterdam, Elsevier, pp. 103–145.
Libourel, G., Krot, A.N., 2007. Evidence for the presence of planetesimal material among the precursors of magnesian chondrules of nebular origin. Earth and Planetary Science Letters 254, 1–8.
Lister, G.F., 1966. The composition and origin of selected iron–titanium deposits. Economic Geology 61, 275–310.
Liu, D., Shen, F.K., Zhang, G.Z., 1985. Layered intrusions of the Panxi area, Sichuan province. In: Zhang, Y.X. (Ed.), Corpus of the Panxi Paleorift Studies in China. Geological Publishing House, Beijing, pp. 85–118.
Luo, Z.-Y., Xu, Y.-G., He, B., Huang, X.-L., Shi, Y.R., 2006. A-type granite and syenite intrusions in Emeishan large igneous provinces: product of the Emeishan plume?

International Conference on Continental Volcanism Abstracts and Program, Guangzhou, China, p. 63.
Ma, Y., Liu, J.F., Wang, H.F., Mao, Y.S., Ji, X.T., Wang, D.K., Yan, Z.Z., 2001. Geology of the Panzhihua Region. Sichuan Science and Technology Press, Chengdu. 367 pp. (in Chinese).
Ma, Y., Ji, X.T., Li, J.C., Huang, M., Kan, Z.Z., 2003. Mineral Resources of the Panzhihua Region. Sichuan Science and Technology Press, Chengdu. 275 pp. (in Chinese).
MacDougall, J.D., 1988. Continental Flood Basalts. Kluwer Academic Publishers, Dordrecht. 341 pp.
Mallmann, G., O'Neill, H.St.C., 2009. The crystal/melt partitioning of V during mantle melting as a function of oxygen fugacity compared with some other elements (Al, P, Ca, Sc, Ti, Cr, Fe, Ga, Y, Zr and Nb). Journal of Petrology 50, 1765–1794.
McDonough, W.F., Sun, S.-S., 1995. The composition of the earth. Chemical Geology 120, 223–253.
Namur, O., Charlier, B., Toplis, M.J., Higgins, M.D., Liégeois, J.-P., Vander Auwera, J., 2010. Crystallization sequence and magma chamber processes in the ferrobasaltic Sept Iles layered intrusion, Canada. Journal of Petrology 51, 1203–1236.
Pang, K.-N., Zhou, M.-F., Lindsley, D.H., Zhao, D., Malpas, J., 2008a. Origin of Fe–Ti oxide ores in mafic intrusions: evidence from the Panzhihua intrusion. Journal of Petrology 49, 295–313.
Pang, K.-N., Li, C., Zhou, M.-F., Ripley, E.M., 2008b. Abundant Fe–Ti oxide inclusions in olivine from the Panzhihua and Hongge layered intrusions, SW China: evidence for early saturation of Fe–Ti oxides in ferrobasaltic magma. Contributions to Mineralogy and Petrology 156, 307–321.
Pang, K.-N., Li, C., Zhou, M.-F., Ripley, E.M., 2009. Mineral compositional constraints on petrogenesis and oxide ore genesis of the Panzhihua layered gabbroic intrusion, SW China. Lithos 110, 199–214.
PXGT (Pan-Xi Geological Team of the Bureau of Geology and Mineral Resources), 1981. Geological Survey Report on the Xinjie V–Ti–Magnetite Ore District in the Miyi county, Sichuan Province, pp. 15–35. in Chinese.
Qi, L., Wang, C.Y., Zhou, M.-F., 2008. Controls on the PGE distribution of Permian Emeishan alkaline and peralkaline volcanic rocks in Longzhoushan, Sichuan Province, SW China. Lithos 106, 222–236.
Qi, L., Zhou, M.-F., 2008. Platinum-group elemental and Sr–Nd–Os isotopic geochemistry of Permian Emeishan flood basalts in Guizhou Province, SW China. Chemical Geology 248, 83–103.
Reynolds, I.M., 1985. Contrasted mineralogy and textural relationships in the uppermost titaniferous magnetite layers of the Bushveld Complex in the Bierkraal area north of Rustenburg. Economic Geology 80, 1027–1048.
Ripley, E.M., Severson, M.J., Hauck, S.A., 1998. Evidence for sulfide and Fe–Ti–P-rich liquid immiscibility in the Duluth Complex, Minnesota. Economic Geology 93, 1052–1062.
Roeder, P.L., Emslie, R.F., 1970. Olivine-liquid equilibrium. Contributions to Mineralogy and Petrology 29, 275–289.
Sandecki, J., 2000. Mineralogical and genetical aspects of the Smalands Taberg Fe–Ti–V ore, Protogine Zone of southern Sweden. GFF 122, 351–358.
SBGMR (Sichuan Bureau of Geology and Mineral Resources), 1991. Regional Geology of Sichuan Province. Geological Memoirs, Series 1, No. 23. Ministry of Geology and Mineral Resources, China. Geological Publishing House, Beijing, 31–35 and 396–403 (in Chinese).
Severson, M.J., 1988. Geology and structure of a portion of the Partidge River intrusion: a progress report. Duluth, University of Minnesota, Natural Resources Research Institute, Technical Report NRRI/GMIN-TR-88-08. 78 pp.
Scoates, J.S., 2000. The plagioclase-magma density paradox re-examined and the crystallization of Proterozoic anorthosites. Journal of Petrology 41, 627–649.
Shellnutt, J.G., Zhou, M.-F., 2007. Permian peralkaline, peraluminous and metaluminous A-type granites in the Panxi district, SW China: their relationship to the Emeishan mantle plume. Chemical Geology 243, 286–316.
Shellnutt, J.G., Zhou, M.-F., Zellmer, G., 2009. The role of Fe–Ti oxide crystallization in the formation of A-type granitoids with implications for the Daly gap: an example from the Permian Baima igneous complex, SW China. Chemical Geology 259, 204–217.
Song, X.-Y., Qi, H.-W., Robinson, P.T., Zhou, M.-F., Cao, Z.-M., Chen, L.-M., 2008. Melting of the subcontinental lithospheric mantle by the Emeishan mantle plume; evidence from the basal alkaline basalts in Dongchuan, Yunnan, Southwestern China. Lithos 100, 93–111.
Tegner, C., Cawthorn, R.G., Kruger, F.J., 2006. Cyclicity in the Main and Upper Zones of the Bushveld Complex, South Africa: crystallization from a zoned magma sheet. Journal of Petrology 47, 2257–2279.
Thompson, G.M., Ali, J.R., Song, X., Jolley, D.W., 2001. Emeishan Basalts, SW China: reappraisal of the formation's type area stratigraphy and a discussion of its significance as a large igneous province. Journal of the Geological Society 158, 593–599.
Toplis, M.J., Corgne, A., 2002. An experimental study of element partitioning between magnetite, clinopyroxene and iron-bearing silicate liquids with particular emphasis on vanadium. Contributions to Mineralogy and Petrology 144, 22–37.
Ukstins Peate, I., Bryan, S.E., 2009. Re-evaluating plume-induced uplift in the Emeishan large igneous province. Nature Geosciences 1, 625–629.
Wang, C.Y., Zhou, M.-F., Qi, L., 2007. Permian flood basalts and mafic intrusions in the Jinping (SW China)–Song Da (northern Vietnam) district: mantle sources, crustal contamination and sulfide segregation. Chemical Geology 243, 317–343.
Wang, C.Y., Zhou, M.-F., Zhao, D., 2008. Fe–Ti–Cr oxides from the Permian Xinjie mafic–ultramafic layered intrusion in the Emeishan large igneous province, SW China: crystallization from Fe- and Ti-rich basaltic magmas. Lithos 102, 198–217.
Xiao, L., Xu, Y.G., Mei, H.J., Zheng, Y.F., He, B., Pirajno, F., 2004. Distinct mantle sources of low-Ti and high-Ti basalts from the western Emeishan large igneous province, SW China: implications for plume–lithosphere interaction. Earth and Planetary Science Letters 228, 525–546.
Xu, Y.G., Chung, S.L., Jahn, B.M., Wu, G.Y., 2001. Petrologic and geochemical constraints on the petrogenesis of Permian–Triassic Emeishan flood basalts in southwestern China. Lithos 58, 145–168.
Zhang, Z., Lu, J., Tang, S., 1999. Sm–Nd ages of the Panxi layered basic–ultrabasic intrusions in Sichuan. Acta Geologica Sinica 73, 263–271 (in Chinese).
Zhang, Z., Mahoney, J.J., Mao, J., Wang, F., 2006. Geochemistry of picritic and associated basalt flows of the western Emeishan flood basalt province, China. Journal of Petrology 47, 1997–2019.
Zhang, Z., Mao, J., Saunders, A.D., Ai, Y., Li, Y., Zhao, L., 2009. Petrogenetic modeling of three mafic–ultramafic layered intrusions in the Emeishan large igneous province, SW China, based on isotopic and bulk chemical constraints. Lithos 113, 369-292.
Zhong, H., Zhu, W.-G., 2006. Geochronology of layered mafc intrusions from the Pan-Xi area in the Emeishan large igneous province, SW China. Mineralium Deposita 41, 599–606.
Zhong, H., Zhou, X.H., Zhou, M.-F., Sun, M., Liu, B.G., 2002. Platinum-group element geochemistry of the Hongge Fe–V–Ti deposit in the Pan-Xi area, southwestern China. Mineralium Deposita 37, 226–239.
Zhong, H., Yao, Y., Hu, S.-F., Zhou, X.-H., Liu, B.G., Sun, M., Zhou, M.-F., Viljoen, M.J., 2003. Trace-element and Sr–Nd isotopic geochemistry of the PGE-Bearing Hongge layered intrusion, Southwestern China. International Geology Review 45, 371–382.
Zhong, H., Yao, Y., Prevec, S.A., Wilson, A.H., Viljoen, M.J., Viljoen, R.P., Liu, B.-G., Luo, Y.-N., 2004. Trace-element and Sr–Nd isotope geochemistry of the PGE-bearing Xinjie layered intrusion in SW China. Chemical Geology 203, 237–252.
Zhong, H., Hu, R.-Z., Wilson, A.H., Zhu, W.-G., 2005. Review of the link between the Hongge layered intrusion and the Emeishan flood basalts, southwest China. International Geology Review 47, 971–985.
Zhong, H., Zhu, W.-G., Chu, Z.-Y., He, D.-F., Song, X.-Y., 2007. Shrimp U–Pb zircon geochronology, geochemistry, and Nd–Sr isotopic study of contrasting granites in the Emeishan large igneous province, SW China. Chemical Geology 236, 112–133.
Zhong, H., Zhu, W.-G., Hu, R.-Z., Xie, L.-W., He, D.-F., Liu, F., Chu, Z.-Y., 2009. Zircon U–Pb age and Sr–Nd–Hf isotope geochemistry of the Panzhihua A-type syenitic intrusion in the Emeishan large igneous province, southwest China and implications for growth of juvenile crust. Lithos 110, 109–128.
Zhou, M.-F., Malpas, J., Song, X.-Y., Robinson, P.T., Sun, M., Kennedy, A.K., Lesher, C.M., Keays, R.R., 2002. A temporal link between the Emeishan large igneous province (SW China) and the end-Guadalupian mass extinction. Earth and Planetary Science Letters 196, 113–122.
Zhou, M.-F., Robinson, P.T., Lesher, C.M., Keays, R.R., Zhang, C.-J., Malpas, J., 2005. Geochemistry, petrogenesis and metallogenesis of the Panzhihua gabbroic layered intrusion and associated Fe–Ti–V oxide deposits, Sichuan Province, SW China. Journal of Petrology 46, 2253–2280.
Zhou, M.F., Arndt, N.T., Malpas, J., Wang, C.Y., Kennedy, A., 2008. Two magma series and associated ore deposit types in the Permian Emeishan large igneous province, SW China. Lithos 103, 352–368.